LOW-FREQUENCY NONUNIFORMITY CORRECTION IN STATIC THERMAL IMAGES

Enrique Sánchez-Monge[1], *Stephanie Lin*[2], *Nicholas Högasten*[2] *and Alessandro Foi*[3,1]

[1]Noiseless Imaging Ltd, Tampere, Finland
[2]FLIR Systems, Goleta (CA), USA
[3]Tampere University of Technology, Tampere, Finland

ABSTRACT

A frequent issue in uncooled thermal cameras is the presence of a low-frequency shading or non-uniformity (NU), where slowly spatially varying changes in intensity corrupt the radiometric image. Usual correction methods for this problem rely on motion in the scene and are therefore unsuitable for static cameras and for restoring individual images. Depending on its physical origin, the NU can be multiplicative, additive, or in-between these two extremes. We propose a static-image demixing method where we separate the low-frequency component causing the NU from the underlying "true" image. Our contribution is three-fold: 1) we propose a parametric transformation that allows a subtractive demixing regardless of the multiplicative or additive nature of the NU; 2) we design a cost functional to evaluate candidate estimates of the NU and of the multiplicative/additive mixing parameter; 3) we propose an iterative method where the NU estimate is progressively updated by optimizing a parametric perturbation with respect to the cost functional. In spite of its simplicity, our method results in a nonparametric NU estimate and a nonlinear demixing. Experiments on simulated and real thermal imagery demonstrates that it successfully removes the low-frequency shading from static scenes. Individual iterations can be also interleaved between frames of a video, allowing for continuous adaptation to changes in the NU.

Index Terms— Non-uniformity, infrared, thermal imaging, demixing.

1. INTRODUCTION

Low-frequency shading is a common problem in infrared (IR) cameras. This type of non-uniformity (NU) in the images can be due to various causes. The shape, size, and position of the housing relative to the lens can result into shading in the corners (e.g., vignetting); when a thermal camera is located near a heat source, such as a heater, a car engine, or direct sunlight, the images produced by the IR camera might have shading in an area that corresponds to the side of the sensor closer to the heat source. Furthermore, some cameras might have imperfect gain correction that results in shading. The low-frequency shading often obscures the actual image content causing loss of perceptible details in the scene.

Conventional NU correction methods are either calibration-based [1, 2, 3], or scene-based [4, 5, 6, 7, 8, 9] that rely on global motion (e.g., panning of the camera) across multiple frames, and may introduce burn-in artifacts when motion is lacking for prolonged periods of time. On the other hand, some single-frame methods tackle only high-frequency components of the NU like column noise [10, 11]. Scene-based methods are not suitable for fixed-mount cameras or for situations where only partial frames are moving (e.g., static surveillance or traffic monitoring cameras). Thus, there is a need for improved NU correction techniques for reducing low-frequency shading from static scenes and single frames.

2. PROPOSED METHOD

The proposed algorithm (patent pending [12]) is intended to separate or *demix* two images – an underlying "true" IR image y and the low-frequency component w causing the NU – from a single frame z. In other words, we do not attempt to remove the high-frequency content of the NU, but only its smooth component.

2.1. Observation Model

Depending on the physical nature of the NU in the image formation, its behaviour can be modeled as additive, multiplicative, or possibly as intermediate between these two. In the additive case, the demixing would be naturally carried out as a subtraction. Interestingly, in the multiplicative case, rather than performing the demixing as a division, one can operate in a logarithmic range and again demix via a subtraction. These facts motivate us to find a way to encompass both cases within a single model and to develop a demixing strategy that can accommodate for both cases, unlike conventional methods that focus on either of these behaviours. To this end, we define a unified image observation model for the image $z : X \to \mathbb{R}$ as

$$z = \mathcal{A}^{-1}\left(e^{\log(\mathcal{A}(y))+w}\right) = \tag{1}$$

$$= \mathcal{A}^{-1}\left(\mathcal{A}(y)\, e^{w}\right) = \tag{2}$$

$$= y e^{w} - \mathcal{A}^{-1}(0)\left(e^{w} - 1\right), \tag{3}$$

where $X \subset \mathbb{Z}^2$ denotes the set of pixel coordinates on which the images z, y, and w are defined, and

$$\mathcal{A}(u) = a_1 u + a_2\,, \qquad \mathcal{A}^{-1}(u) = \frac{u - a_2}{a_1}\,, \qquad u \in \mathbb{R}, \tag{4}$$

are an affine transformation of the image intensities and its inverse.

The mixing with w described by (1)-(3) can be additive or multiplicative, depending on the coefficients a_1, a_2. It is clear from (3) that for $\frac{a_2}{a_1} = 0$ (linear $\mathcal{A}$) we have a multiplicative NU as the product of y by e^w. Multiplicative NU can occur also modulo a generic affine transformation, as in (2). The additive NU case can be appreciated from the Maclaurin expansion of (3) with respect to w,

$$z = y + \left(\frac{a_2}{a_1} + y\right)\left(w + \frac{w^2}{2} + \frac{w^3}{6} + \dots\right), \tag{5}$$

which becomes $z \approx y + \frac{a_2}{a_1} w$ for $\left|\frac{a_2}{a_1}\right| \gg |y|$. This condition can be interpreted as the range of $\mathcal{A}(y)$ being distributed over an interval where the curvature of the logarithm is negligible, i.e. where $\log$ can

be treated as an affine mapping. Thus, $\mathcal{A}$ controls the degree of multiplicative or additive behavior of the NU.

The identities (1)-(2) formalize how these different types of NU can all be expressed in additive form through a logarithm. Specifically, we can define the transformed image as

$$\tilde{z} = \log\left(\mathcal{A}(z)\right) = \log\left(\mathcal{A}(y)\right) + w\,, \tag{6}$$

and demix by estimating w and subtracting it from $\tilde{z}$.

2.2. Normalization to unit range

For numerical purposes, it is convenient to recast the above model with respect to an image normalized to the $[0, 1]$ range of intensities. Let us denote by

$$\mathcal{N}_z(u) = \frac{u - \min_X\{z\}}{\max_X\{z\} - \min_X\{z\}}\,, \qquad u \in \mathbb{R}\,,$$
$$\mathcal{N}_z^{-1}(u) = u\left(\max_X\{z\} - \min_X\{z\}\right) + \min_X\{z\}\,, \qquad u \in \mathbb{R}\,,$$

the forward and inverse normalization operators respectively, and let $\bar{z} = \mathcal{N}_z(z)$. Then, $\tilde{z}$ (6) can be rewritten as

$$\tilde{z} = \log\left(\mathcal{A}\left(\mathcal{N}_z^{-1}(\bar{z})\right)\right) = \log\left(c_1\bar{z} + c_2\right), \tag{7}$$

where the coefficients of the composition of $\mathcal{A}$ and $\mathcal{N}_z^{-1}$ are

$$c_1 = a_1(\max_X\{z\} - \min_X\{z\}), \qquad c_2 = a_2 + a_1 \min_X\{z\}\,. \tag{8}$$

We can then normalize $\tilde{z}$ (7) to the $[0, 1]$ range as

$$\mathcal{N}_{\tilde{z}}(\tilde{z}) = \frac{\log\left(c_1\bar{z} + c_2\right) - \log\left(c_2\right)}{\log\left(c_1 + c_2\right) - \log\left(c_2\right)} = \frac{\log\left(\frac{c_1}{c_2}\bar{z} + 1\right)}{\log\left(\frac{c_1}{c_2} + 1\right)}\,. \tag{9}$$

2.3. Parametric transformation

Based on the above, we process normalized frames $\bar{z} = \mathcal{N}_z(z)$ through the parametric transformation $f_q : [0, 1] \to [0, 1]$, $q \in \mathbb{R}$, defined as

$$f_0(u) = u\,, \qquad f_q(u) = \frac{\log\left(q^2u + 1\right)}{\log\left(q^2 + 1\right)}, \quad q \neq 0\,. \tag{10}$$

Applying f_q to $\bar{z}$ is equivalent to mapping the range of z onto a portion of the logarithmic curve, as determined by the parameter q, which thus controls the degree between additive and multiplicative behaviour of the NU. In particular, if $q^2 = \frac{c_1}{c_2}$ then $f_q(\bar{z}) = \mathcal{N}_{\tilde{z}}(\tilde{z})$ (9), which means that the transformation f_q (10) can reproduce (6) for any given $\mathcal{A}$, provided a suitable choice of $q \in \mathbb{R}$. From Figure 1 it can be seen that the transformation approaches linearity as $|q| \to 0$, which by (8) corresponds to $\left|\frac{a_2}{a_1}\right| \to +\infty$, thus enabling the additive behavior of the NU as per (5).

Our approach is then to perform the signal demixing as the subtraction $f_q(\bar{z}) - v$, for a choice of q that makes the NU additive. Thereafter the image is transformed back into the linear range by inverting (10),

$$f_0^{-1}(u) = u\,, \qquad f_q^{-1}(u) = \frac{e^{u\log\left(q^2+1\right)} - 1}{q^2}, \quad q \neq 0\,,$$

and then to the original range by $\mathcal{N}_z^{-1}$. Indeed, if $v = \mathcal{N}_{\tilde{z}}(w)$ and $q^2 = \frac{c_1}{c_2}$,

$$\mathcal{N}_z^{-1}\Big(f_q^{-1}\left(f_q(\bar{z}) - v\right)\Big) = y\,. \tag{11}$$

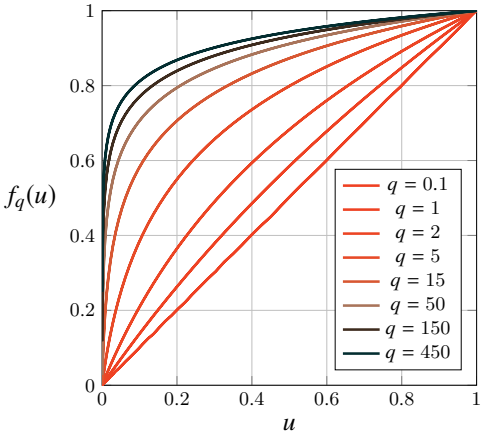

Fig. 1. Parametric transformation f_q (10) for different values of the parameter q.

2.4. Algorithm

In general, separating the NU from an image is an under-determined problem which in principle can have infinite arbitrary solutions. Some constraints must be introduced in order to obtain a meaningful and stable solution. For this purpose, we make the following assumptions:

1. an ideal noise-free IR image is typically piecewise flat;
2. the NU is smooth, without sharp transitions or edges.

These conditions aim at removing only the low-frequency shading, without affecting image details or the low-frequency content of the underlying scene. They provide us with the design of a cost functional whose minimum corresponds to a suitable solution of the demixing problem. Specifically, to promote the piecewise regularity of the demixed image, we want its total variation (TV) semi-norm to be small, i.e. we aim at minimizing the ℓ_1-norm of its gradient. Secondly, to promote the smoothness of the NU, we attempt to minimize the ℓ_2-norm of the Laplacian of v. It is clear that it is not possible to minimize both to zero simultaneously, therefore the solution must find a balance between them. Consequently, we define the cost functional as

$$\mathcal{F}_{\bar{z}}(q, v) = \mathcal{TV}^2\Big(f_q\left(\bar{z}\right) - v, f_q'\left(\bar{z}\right)\Big) + \lambda\,\mathcal{E}^2\left(v, f_q'\left(\bar{z}\right)\right), \tag{12}$$

where

$$\mathcal{TV}(u, h) = \frac{1}{n}\left\|\frac{\nabla u}{h}\right\|_1, \qquad \mathcal{E}^2(u, h) = \frac{1}{n}\left\|\frac{\Delta u}{h}\right\|_2^2$$

are, respectively, the TV semi-norm and the energy of the Laplacian, and n is the number of pixels in the image. The parameter λ is used to balance the two addends in (12). We scale the gradient and Laplacian in (13) by the derivative of the transformation function, $f_q'(\bar{z})$, in a pixelwise manner; this is done in order to minimize the quantitative influence of the slope of f_q onto the cost functional (12).

We propose a greedy iterative algorithm that uses a series of simple parametric perturbations to estimate v by minimizing the cost functional (12). Specifically, at each iteration, we optimize both the transformation parameter q and a parameter vector $\mathbf{p}$ of a parametric

perturbation $\mathbf{\Pi}_{k_i}$ of the past estimate $\hat{v}_{i-1}$ of $v = \mathcal{N}_{\bar{z}}(w)$:

$$\hat{q}_i, \hat{\mathbf{p}}_i = \arg\min_{q,\mathbf{p}} \mathcal{F}_{\bar{z}}\left(q, \mathbf{\Pi}_{k_i}(\mathbf{p}, \hat{v}_{i-1})\right), \tag{13}$$
$$\hat{v}_i = \mathbf{\Pi}_{k_i}(\hat{\mathbf{p}}_i, \hat{v}_{i-1}).$$

We alternate between three parametric perturbations ($k_i \in \{1, 2, 3\}$). The first perturbation type consists in the addition of 2D Gaussian function, or *bump*,

$$\mathbf{\Pi}_1([\alpha, \mathbf{x}], v) = v + \alpha \mathbf{G}_{[\mathbf{x}, \sigma_G]}, \tag{14}$$

where $\mathbf{G}_{[\mathbf{x},\sigma_G]}$ is a 2D Gaussian function with standard deviation (width) σ_G centered at position $\mathbf{x} \in \mathbb{R}^2$. The signed amplitude is controlled by $\alpha \in \mathbb{R}$. Only α and $\mathbf{x}$ are optimized, while σ_G is randomly selected at each iteration, but always larger than a fixed constant $\sigma_{\min}$ that determines the maximum bandwidth of the NU. The second type of perturbation is a global smoothing,

$$\mathbf{\Pi}_2(\mu, v) = (1 - \mu)\, v + \mu\, \Upsilon(v), \tag{15}$$

where Υ is a smoothing operator and $\mu \in [0, 1]$. A new v is obtained as a convex combination between the old v and a smoothed version of itself. In order to adapt to changes in q, a global response operation is introduced, where a new v is obtained as a polynomial of the old v. This third perturbation type is modeled as

$$\mathbf{\Pi}_3([s_1, s_2], v) = s_2 v^2 + s_1 v. \tag{16}$$

Thus, for these three perturbation types, the parameter vector $\mathbf{p}$ in (13) belongs to $\mathbb{R}^3$, $\mathbb{R}$, and $\mathbb{R}^2$, respectively, making the minimization feasible with standard methods such as the Nelder-Mead downhill simplex algorithm [13].

After each iteration, an estimate $\hat{y}_i$ of the image y can be obtained from $\hat{q}_i$ and $\hat{v}_i$ (13) via (11) as

$$\hat{y}_i = \mathcal{N}_z^{-1}\left(f_{\hat{q}_i}^{-1}(f_{\hat{q}_i}(\bar{z}) - \hat{v}_i)\right).$$

Although each iteration involves a simple parametric model, the estimate of v resulting from a multitude of iterations is effectively nonparametric, as the perturbations are cascaded.

2.4.1. *Numerical precision*

To prevent round-off errors, one can approximate f_q and f_q^{-1} for small q (e.g., $|q| \leq 0.1$ for single floats) as

$$f_q(u) \approx \frac{u\left(2q^4u^2 - 3q^2u + 6\right)}{2q^4 - 3q^2 + 6},$$
$$f_q^{-1}(u) \approx \frac{q^4u\left(u^2 - 3u + 2\right)}{6} + \frac{q^2u(u-1)}{2} + u,$$

whereas for large q (e.g., $|q| \geq 10^{19}$ for single floats), setting $p = 2\log(q)$,

$$f_q(u) \approx \frac{\log(u(1 - e^{-p}) + e^{-p})}{p} + 1,$$
$$f_q^{-1}(u) \approx \frac{e^{-p(1-u)} - e^{-p}}{1 - e^{-p}}.$$

3. EXPERIMENTS

We validate our demixing algorithm on artificial as well as real long-wavelength IR (LWIR) images. For all experiments we fix $\lambda = 50$ and let the algorithm run for 10^4 iterations. We set the bandwidth parameter $\sigma_{\min} = 0.25H$, where H is the image height in pixels, except for the experiments in Section 3.2.1, where we illustrate the results for different values of $\sigma_{\min}$.

In the figures, all images are visualized individually normalized to their range prior (black and white respectively being the minimum and maximum attained value).

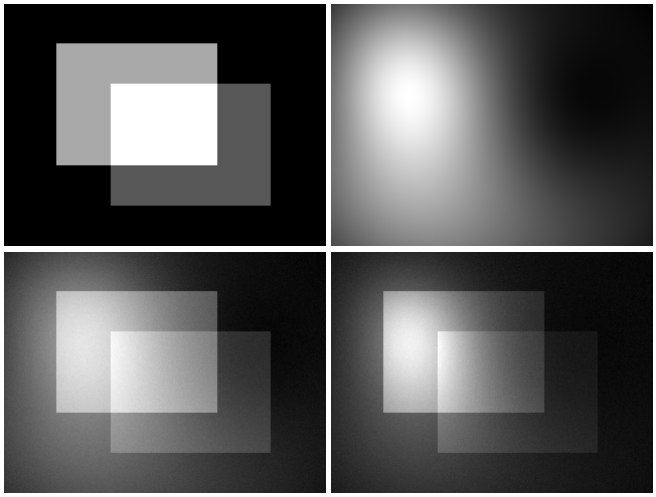

Fig. 2. Artificial examples of images corrupted by NU. Top-left: ground truth y. Top-right: smooth function ω. Bottom-left: image corrupted by an additive NU and additive white Gaussian noise, $z = y + \omega + \eta$. Bottom-right: image corrupted by a multiplicative NU and additive white Gaussian noise, $z = ye^{\omega} + \eta$. The relative standard deviation of the noise η is 1% in both cases.

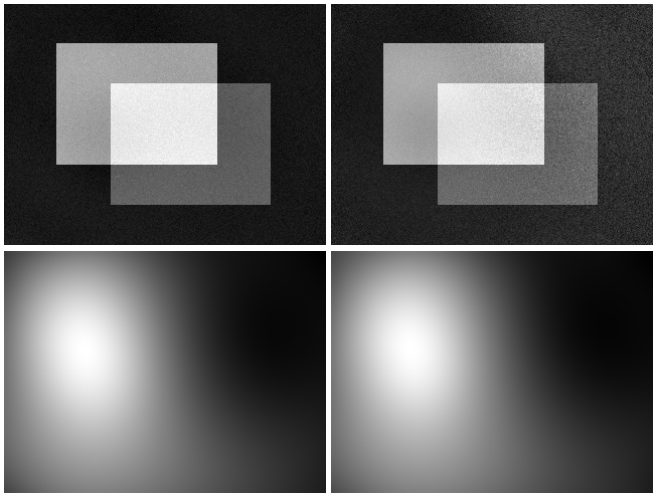

Fig. 3. Results of applying the proposed demixing algorithm to the images at the bottom of Figure 2: Estimated $\hat{y}$ (top) and $\hat{v}$ (bottom) from the additive (left) and multiplicative (right) cases, respectively.

3.1. Artificial images

Given a piecewise constant test image y and a smooth function ω, we generate observations corrupted by additive and multiplicative NU respectively as $z = y + \omega + \eta$ and $z = ye^{\omega} + \eta$, where η is additive

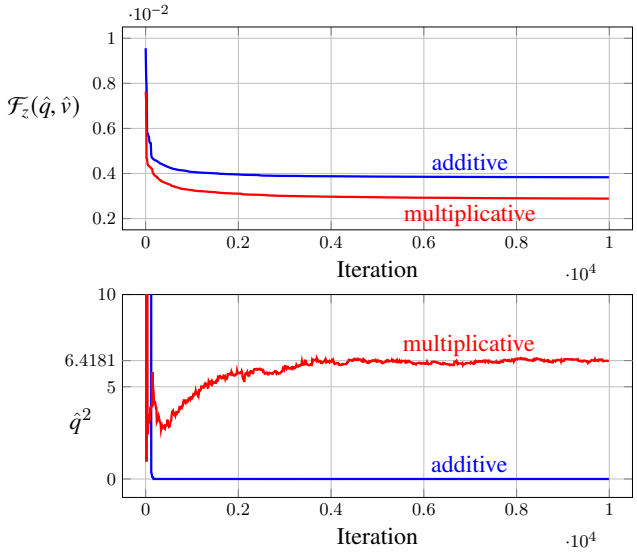

Fig. 4. Evolution of the proposed algorithm on the artificial examples for the additive (blue) and multiplicative (red) cases shown at the bottom of Figure 2. It can be seen how the algorithm eventually determines the additive or multiplicative nature of the NU, with $\hat{q}^2$ respectively approaching the ground-truth values of 0 or 6.4181.

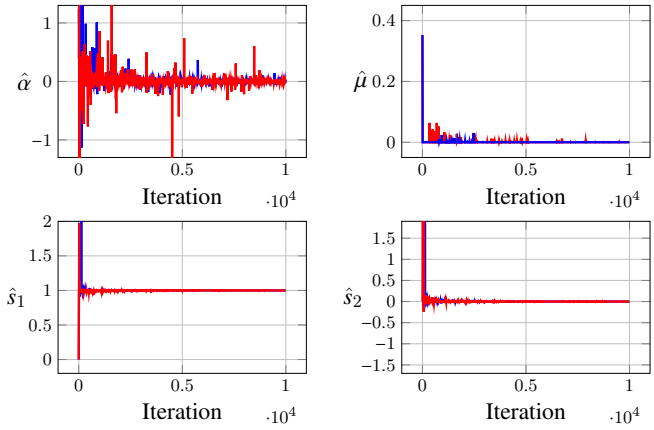

Fig. 5. Optimized perturbation parameters at each iteration for the examples at the bottom of Figure 2; blue and red plots respectively correspond to the additive and to the multiplicative case. Top-left: signed amplitude α of the 2D Gaussian function of $\mathbf{\Pi}_1$ (14) ($\mathbf{x}$ not shown). Top-right: $\mathbf{\Pi}_2$ smoothing perturbation parameter μ (15). Bottom: $\mathbf{\Pi}_3$ polynomial perturbation parameters s_1, s_2 (16).

white Gaussian noise with a relative standard deviation of 1%. The corresponding images are shown in Figure 2. Neglecting the noise η, the observation model of Section 2 holds as follows. For the additive case, based on (5), we have $\omega = \frac{a_2}{a_1} w$ with an infinitely large $\frac{a_2}{a_1}$ and an infinitely small w, which by (8) implies $q^2 = 0$, i.e. a linear f_q. For the multiplicative case, by (2)-(3) we have $\omega = w$, $a_2 = 0$, and $a_1 \neq 0$; the specific range of z yields via (8) $q^2 = 6.4181$. Note that in both cases ω, w, and $v = \mathcal{N}_{\bar{z}}(w)$ coincide upon normalization.

The results of the algorithm are shown in Figure 3: in both cases the algorithm effectively corrects the NU, providing accurate estimates $\hat{y}$ and $\hat{v}$ of y and v, respectively. Observe that $\hat{y}$ remain noisy, as the procedure does not attempt to remove noise. Figures 4 and 5 show the evolution of the cost $\mathcal{F}_z(\hat{q},\hat{v})$, of $\hat{q}^2$, and of the perturbation parameters across the iterations, demonstrating convergence to the ideal value of q^2 and vanishing of the perturbations.

3.2. Real LWIR imagery

We applied the proposed algorithm to static LWIR images where the low-frequency NU is a common issue. The results are shown in Figure 6 and demonstrate an effective removal of the low-frequency NU, even in cases where the NU dominates over the image. Note how the corrected images feature increased contrast and detail.

3.2.1. Influence of the bandwidth parameter

The selection of the maximum bandwidth of the 2D Gaussian perturbations, determined by $\sigma_{\min}$, is important for the effectiveness of the demixing. As shown in Figure 7, a very small bandwidth prevents the correction of the NU whereas a too large bandwidth results in image content being treated as part of the NU.

4. CONCLUSIONS

We have proposed an image observation model that is able to encompass both multiplicative and additive NU. The model is linked to a parametric nonlinear transformation that permits the subtractive removal of the NU regardless of its original nature. Furthermore, we have designed a cost functional that provides means to evaluate candidate estimates and mixing models of the NU. Finally, we have demonstrated the effectiveness of a greedy iterative update by a series of low-dimensional parametric perturbations that allow the minimization of the proposed cost functional. Experiments on artificial test images and on real LWIR images show that the proposed approach identifies the unknown mixing model and effectively corrects the low-frequency NU.

Although the NU estimation may possibly be approached as a diffusion problem [14], our implementation through the parametric perturbations has the advantage of directly integrating the adaptive selection of q and an explicit definition of the bandwidth $\sigma_{\min}$.

The presented algorithm is naturally applicable to video. We remark that only the estimates of v and q are passed to the next iteration, which can thus be carried out with a new frame z. Therefore, individual (or a few) iterations can be interleaved between frames and the process can operate continuously, adapting to the possible variations of the NU over time.

While in this work we focused on infrared imaging, the proposed approach may prove useful to many other modalities affected by NU problems, e.g., magnetic-resonance imaging, where the low-frequency NU is known as bias field or inhomogeneity [15].

5. REFERENCES

[1] B. M. Ratliff, M. M. Hayat, and J. S. Tyo, "Radiometrically accurate scene-based nonuniformity correction for array sensors," *J. Opt. Soc. Am. A*, vol. 20, no. 10, pp. 1890–1899, Oct 2003.

[2] A. Wolf, J. E. Pezoa, and M. Figueroa, "Modeling and compensating temperature-dependent non-uniformity noise in IR microbolometer cameras," *Sensors*, vol. 16, no. 7, 2016.

[3] H. Budzier and G. Gerlach, "Calibration of uncooled thermal infrared cameras," *J. Sensors and Sensor Sys.*, vol. 4, no. 1, pp. 187–197, 2015.

[4] D. A. Scribner, K. A. Sarkady, J. T. Caulfield, M. R. Kruer, G. Katz, C. Gridley, and C. Herman, "Nonuniformity correction for staring IR focal plane arrays using scene-based techniques," in *Proc. SPIE Infrared Detectors and Focal Plane Arrays*, vol. 1308, 1990, pp. 224–234.

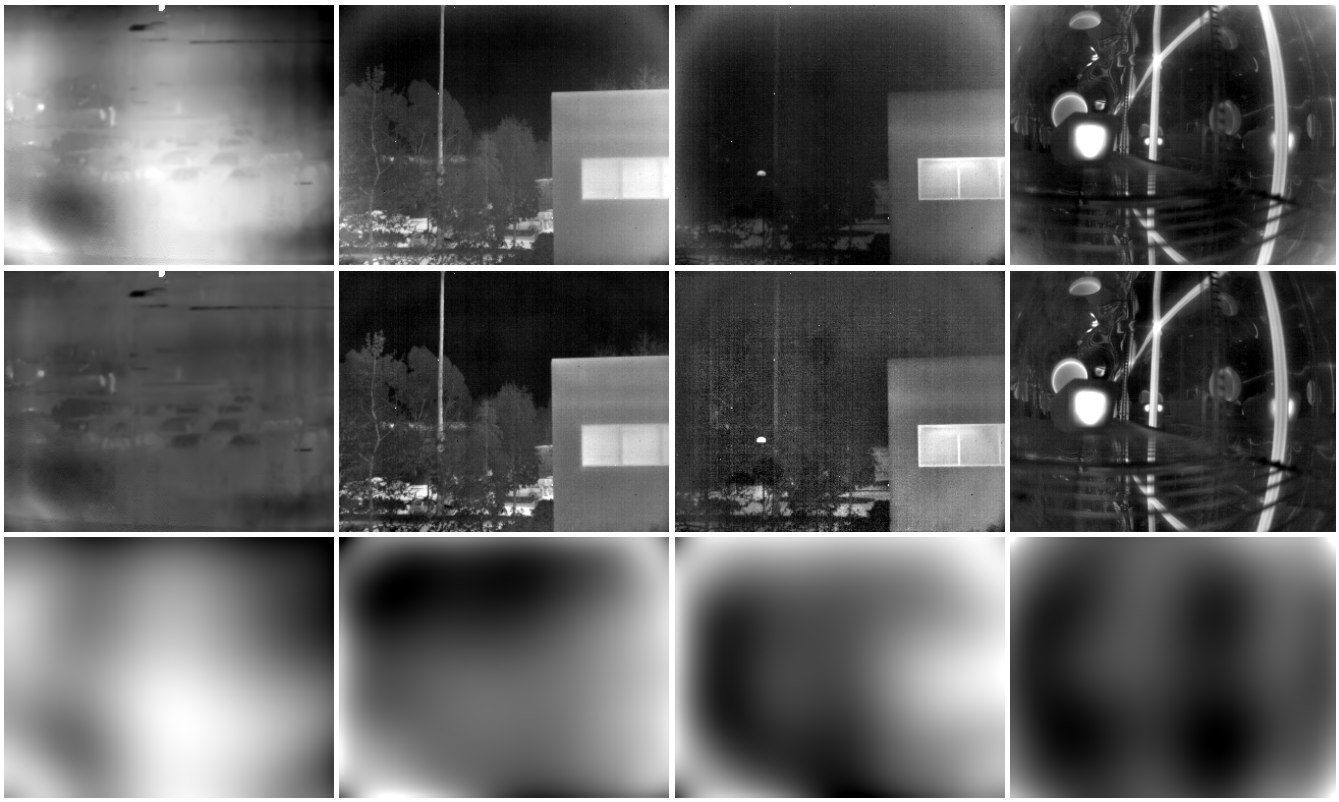

Fig. 6. Top: original LWIR images z. Middle: corrected images $\hat{y}$. Bottom: estimated $\hat{v}$.

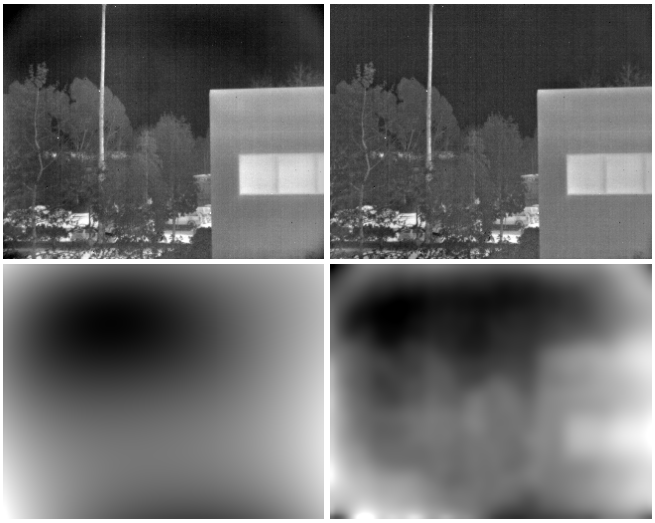

Fig. 7. Effect of the bandwidth on the NU estimates using respectively a bandwidth 8 times smaller ($\sigma_{\min} = 2H$, left) and 8 times larger ($\sigma_{\min} = 0.0312H$, right) than used in all other experiments. Top: corrected images $\hat{y}$. Bottom: estimated $\hat{v}$. If the bandwidth is too permissive (right) image content leaks into $\hat{v}$, while a too restrictive bandwidth (left) might not be enough for a complete removal of the NU (see, e.g., the corners of $\hat{y}$ and $\hat{v}$).

[5] D. A. Scribner, K. A. Sarkady, M. R. Kruer, J. T. Caulfield, J. Hunt, and C. Herman, "Adaptive nonuniformity correction for IR focal-plane arrays using neural networks," in *Proc. SPIE Infrared Sensors: Detectors, Electronics, and Signal Processing*, vol. 1541, 1991, pp. 100–110.

[6] J. G. Harris and Y.-M. Chiang, "Nonuniformity correction of infrared image sequences using the constant-statistics constraint," *IEEE Trans. Image Process.*, vol. 8, no. 8, pp. 1148–1151, 1999.

[7] R. C. Hardie, M. M. Hayat, E. Armstrong, and B. Yasuda, "Scene-based nonuniformity correction with video sequences and registration," *Applied Optics*, vol. 39, no. 8, pp. 1241–1250, 2000.

[8] S. N. Torres, E. M. Vera, R. A. Reeves, and S. K. Sobarzo, "Adaptive scene-based nonuniformity correction method for infrared-focal plane arrays," in *Proc. SPIE Infrared Imaging Systems: Design, Analysis, Modeling, and Testing XIV*, vol. 5076, 2003, pp. 130–140.

[9] C. Zuo, Q. Chen, G. Gu, and X. Sui, "Scene-based nonuniformity correction algorithm based on interframe registration," *J. Opt. Soc. Am. A*, vol. 28, no. 6, pp. 1164–1176, 2011.

[10] Y. Tendero, J. Gilles, S. Landeau, and J. Morel, "Efficient single image non-uniformity correction algorithm," in *Proc. SPIE Security + Defence 2010*, vol. 7834, Electro-Optical and Infrared Systems: Technology and Applications VII, 2010.

[11] Y. Tendero, S. Landeau, and J. Gilles, "Non-uniformity Correction of Infrared Images by Midway Equalization," *Image Processing On Line*, vol. 2, pp. 134–146, 2012.

[12] E. Sánchez-Monge and A. Foi, "Systems and Methods for Reducing Low-Frequency Non-Uniformity in Images," US Patent Application 62/471,854 filed March 15, 2017; WIPO WO/2018/170171.

[13] A. R. Conn, K. Scheinberg, and L. N. Vicente, *Introduction to derivative-free optimization*. SIAM, 2009.

[14] O. Scherzer, M. Grasmair, H. Grossauer, M. Haltmeier, and F. Lenzen, *Variational methods in imaging*. Springer, 2009.

[15] N. J. Tustison, B. B. Avants, P. A. Cook, Y. Zheng, A. Egan, P. A. Yushkevich, and J. C. Gee, "N4ITK: Improved N3 bias correction," *IEEE Trans. Medical Imaging*, vol. 29, no. 6, pp. 1310–1320, 2010.